Solid State Communications 288 (2019) 33–37

Contents lists available at ScienceDirect

Solid State Communications

journal homepage: www.elsevier.com/locate/ssc

Communication

Structural and electronic properties of BiOF with two-dimensional layered structure under high pressure: Ab initio study

Mehmet Canpolat[a], Cihan Kürkçü[b,*], Çağatay Yamçıçıer[a], Ziya Merdan[c]

[a] Institute of Science, Gazi University, 06500, Ankara, Turkey
[b] Department of Electronics and Automation, Ahi Evran University, 40100 Kırşehir, Turkey
[c] Science Faculty, Gazi University, 06500, Ankara, Turkey

ARTICLE INFO

Communicated by Julie Staunton

Keywords:
Intermediate phase
Phase transition
Enthalpy
Electronic structure

ABSTRACT

In this work, the crystal structure of the BiOF is studied under high hydrostatic pressure using ab initio calculations. Pressure-volume relationships and structural transitions are investigated using Siesta method. A first-order phase transition from the tetragonal matlockite PbFCl-type structure with space group P4/nmm to the orthorhombic structure with space group Cmcm is successfully observed for BiOF. This phase transition which occur around 19.6 GPa is also analyzed from the total energy and enthalpy calculations. In addition, electronic properties of BiOF are researched during the pressure. By analyzing the energy band structures, it is found that the band gaps P4/nmm and Cmcm phases for the BiOF are 2.74 and 2.47 eV, respectively.

1. Introduction

Recently, many efforts have been made to develop new photocatalysts such as nitrides, sulfides, oxynitrides, oxysulfides and oxyhalides. Among these photocatalysts, bismuth oxyhalides with perfect layered structure (Bi*OX*, *X* = F, Cl, Br, I) have attracted much attention in the fields of removal of heavy metal ions, sterilization, photocatalytic degradation of organic pollutants [1–9], cosmetics [10], solar cells [11] and photoelectron chemical devices [12].

Due to its unique chemical and physical features such as electrical, mechanical and structural features et al., the perfect layered structure (two-dimensional (2D)) of bismuth oxyhalides have been attracted many researchers because they are preferred both theoretical and experimental aspects [13–15].

Particularly, the separation of photo-induced electron–hole pairs are favored by the perfect layered structure. So bismuth oxyhalides display perfect photocatalytic activity. Until now, innumerable theoretical and experimental works have concentrated on the perfect layered structures and their unique photocatalytic activity of bismuth oxyhalides [16–25].

BiOF crystallizes in a tetragonal matlockite (PbFCl)-type structure of space group P4/nmm (with Bi atoms at the 2c (1/4, 1/4, z) Wyckoff position, where z = 0.212410, O atoms at the 2a (3/4, 1/4, 0) position and F atoms at the 2c (1/4, 1/4, z) position, where z = 0.674669) with six atoms in the crystal cell at ambient conditions. BiOF contains two molecules and its lattice parameters are $a = b = 3.7343$ Å, $c = 6.4168$ Å and $\alpha = \beta = \gamma = 90^{\circ}$.

Zhou et al. [26] firstly explored the high pressure phases of BiOF using the ab initio evolutionary methodology. At the same time, they discussed the phase transition mechanism of BiOF under pressure. They simulated a phase transition from the P4/nmm to the Cmcm phase by means of Born-Oppenheimer Molecular Dynamics using the CASTEP code. At higher pressures, they found that Cmcm structure becomes stable and so believe P4/nmm phase may transform to Cmcm phase directly. They also calculated electronic properties ofBiOF and obtained band gap of 2.50 eV for the Cmcm phase. This band gap value is in good agreement with our result (2.47 eV). At high pressure, we obtained phase transition from the P4/nmm to the Cmcm phase directly. This result is in good agreement with Zhou et al.'s predictions.

The properties of structural and electronic including band structures and densities of states of BiOF crystal are discussed in detail. The calculated results could be beneficial for understanding the photocatalytic properties and mechanism of BiOF crystal [2,6,22,23].

2. The method of calculations

The phase transition properties of the tetragonal PbFCl-type structure of BiOF under pressure are investigated using the ab initio method. The SIESTA [27] package program is used as the ab-initio code in the study. Generalized Gradient Approximation (GGA) is applied and parameters of the Perdew-Burke-Ernzerhof (PBE) [28] exchange-correlation function are entered into the calculations with "double ζ (DZ)

* Corresponding author. (C. Kürkçü).
E-mail address: ckurkcu@ahievran.edu.tr (C. Kürkçü).

https://doi.org/10.1016/j.ssc.2018.11.010
Received 29 August 2018; Received in revised form 10 November 2018; Accepted 13 November 2018
Available online 14 November 2018
0038-1098/

basis set". Troullier-Martins' norm-conserving pseudo-potential [29] is used for electronic band structure, total and partial density of state calculations. Cut off energy at this study was sufficient as 300 Ryd to represent the electron density, the local part of the pseudopotentials, as well as the Hartree and the exchange-correlation potential. In order to calculate the relationship between the energy and volume, the unit cells of the crystal structures are utilized for P4/nmm and Cmcm phases. For Brillouin region integration, $10 \times 10 \times 6$ and $12 \times 4 \times 12$ Monkhorst-Pack (MP) mesh [30] were used for the P4/nmm and Cmcm structures, respectively.

Simulation cells were constructed by a $3 \times 3 \times 2$ supercell including 108 atoms under periodic bond conditions. The simulation was carried out starting a zero pressure and the pressure of the system was gradually increased by 10 GPa. At every pressure rise, the system was relaxed to get its equilibrium volume and lowest energy. To get optimized lattice vectors and atomic positions, the stress tolerance and maximum atomic force was taken less than 0.5 GPa and smaller than 0.01 eV $Å^{-1}$, respectively. In addition, to minimize the geometries, a Conjugate-Gradient technique was used under a constant pressure and calculations was achieved at zero kelvin temperature.

The KPLOT [31] program and the RGS [32] algorithm were used to analyze each minimization step. They give detailed information about the space group, atomic positions and lattice parameters of the studied structure. In addition, the CrystalMaker program is used to visualize phase transformation and its mechanism.

3. Results and discussions

Firstly, BiOF are equilibrated by relaxing 108 atoms supercell at zero pressure. The equilibrium unit cell lattice constants are found to be $a = b = 3.7343$ Å, $c = 6.4168$ Å for PbFCl-type structure of BiOF. The phase transition, equilibrium lattice parameters, bulk modulus and pressure derivatives of BiOFat 0 GPa are tabulated in Table 1. Later, the phase transition properties for BiOFare investigated under constant pressure. The pressure-volume relation is shown Fig. 1. A sharp decrease in volume is observed because of the variation of the pressure from 50 GPa to 60 GPa for BiOF. It is clear that the change in volume is discontinuous at the transition pressure, characterizing the first-order nature.

Fig. 2 shows that tetragonal PbFCl-type structure with space group P4/nmm of BiOF converts into an orthorhombic structure with space group Cmcm at 60 GPa. From the results, one can conclude that phase transitions of BiOF under pressure can be reliably predicted based on ab initio calculations. However, the predicted phase transition pressures give slightly different results comparing with the experimental results. The reason of this differences is related to the infinite volume defect form of free structure where the phase transition occurs over the whole simulation cell rather than nucleation and buildup. Therefore, such an overestimated transition pressure can be predicted for the particular

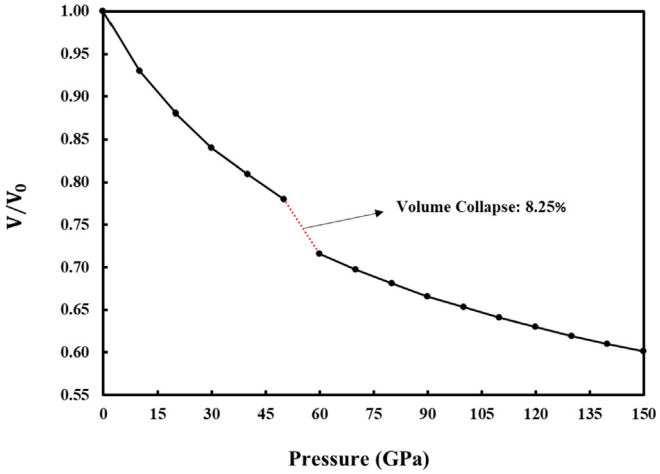

Fig. 1. (Color online) The graph of the change of simulation cell volume as function of the pressure.

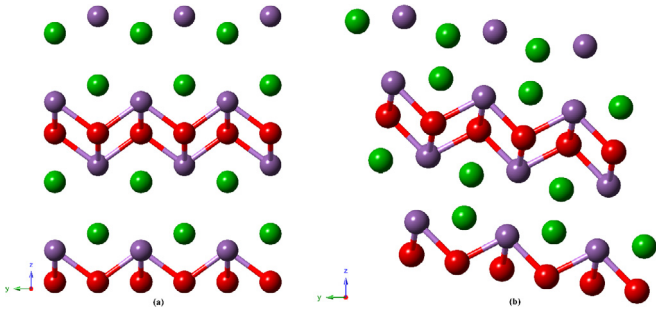

Fig. 2. (Color online) Crystal structures ofBiOF: (a) P4/nmm and (b) Cmcm.

conditions such as finite size of the simulation cell and the time scale of simulations, etc. [33–36] On the other hand, energy-volume calculations (see Fig. 3) are considered to find out the stability of P4/nmmand Cmcm phases, since the thermodynamic theorem does not consider the possible an activation energy barrier separating the two structural phases. As can be seen in Fig. 3, the most stable phase of BiOF is P4/nmm.

Their energy-volume data is fitted to the third-order Birch-Murnaghan equation of state [37,38] that given by

$$P = 1.5B_0\left[\left(\frac{V}{V_0}\right)^{-\frac{7}{3}} - \left(\frac{V}{V_0}\right)^{-\frac{5}{3}}\right] \times \left\{1 + 0.75\left(B_0^{'} - 4\right)\left[\left(\frac{V}{V_0}\right)^{-\frac{2}{3}} - 1\right]\right\} \quad (1)$$

where P is the pressure, Vis the volume at the pressure, V_0, B_0 and $B_0^{'}$ are the volume, bulk modulus and its pressure derivative at 0 GPa, respectively.

Table 1
Theoretical (T = 0 K) lattice parameters of BiOF for PbFCl structure (space group, SG: P4/nmm) and high-pressure phases: Orthorhombic structure (SG: Cmcm) with GGA at the corresponding pressure P_T. *a*, *b*, and *c* are the lattice parameters, V is the equilibrium volume at the respective pressure, B_0 the bulk modulus, $B_0^{'}$ the first derivative of the bulk modulus.

Phases	P_T (GPa)	*a* (Å)	*b* (Å)	*c* (Å)	V (Å^3)	B_0 (GPa)	$B_0^{'}$	References
P4/nmm	0	3.7343	3.7343	6.4168	89.48	81.70	3.68	This study
		3.7940	3.7940	6.2280				[39]
		3.7710	3.7710	6.2750	89.20			[40]
		3.7480	3.7480	6.2240				[41]
		3.7880	3.7880	6.1980				[42]
		3.6310	3.6310	6.2300				[43]
		3.7650	3.7650	6.1630				[44]
		3.7200	3.7200	6.2000				[45]
Cmcm	19.6	3.5059	10.2576	3.5625	128.12	68.67	3.60	This study
		3.0471	8.7839	3.1305				[26]

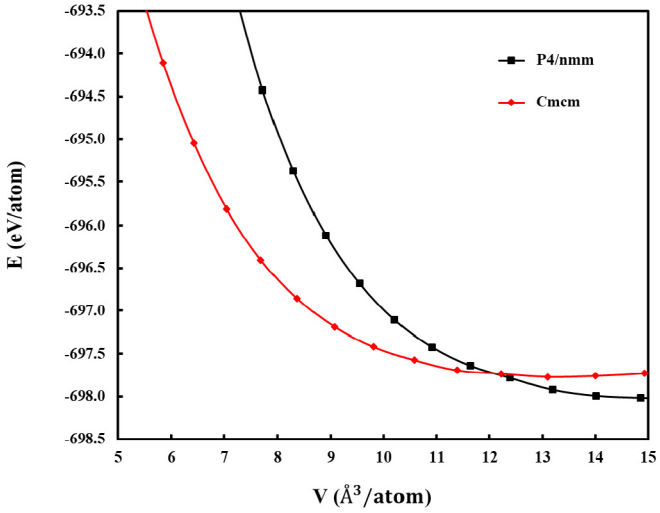

Fig. 3. (Color online) The energy-volume curves of main structural phases ofBiOF.

Enthalpy (H)is the sum of the total energy (E_{tot})and the product of pressure and volume (PV) given by the equation:

$$H = E_{tot} + PV \quad (2)$$

where $P = dE_{tot}/dV$is obtained by differentiation of the predicted the energy-volume curves. Therefore, the transition pressure can be calculated by equating the enthalpy of the two pressure (see Fig. 4). The transition pressures about 19.6 GPa are obtained as P4/nmm → Cmcm in BiOF.

The variation of simulation cell under the pressure gives information about this transformation. The simulation box is initially a cubic cell whose lattice vectors are along the [0 0 1], [0 1 0] and [0 0 1] directions. Thus, as based on predicted parameters, we analyzed the variation of the simulation cell lengths and angles as a function of minimization step (see Fig. 5).

From Fig. 5(a), the α, β and γ (about 90°) angles remain constant up to about 25th minimization step. Then the α and β angles start to increase at around 50th minimization step and after reaching about95°, they remain unchanged through the whole simulation. The γ angle starts to decrease at around 50th minimization step and after reaching67°, it remains unchanged through the whole simulation.

From Fig. 5(b), The *A*, *B* and *C* also remain constant up to about 25th minimization step. Then the *A* and *B* lengths start to increase up to around 50th minimization step and after reaching about11 Å, they start to decrease up to about 10.5 Å. After that they remain unchanged through the whole simulation. The *C* length starts to decrease at around 50th minimization step and after reaching9.8 Å, it starts to increase up to around 10.7 Å. Then it remains unchanged through the whole simulation.

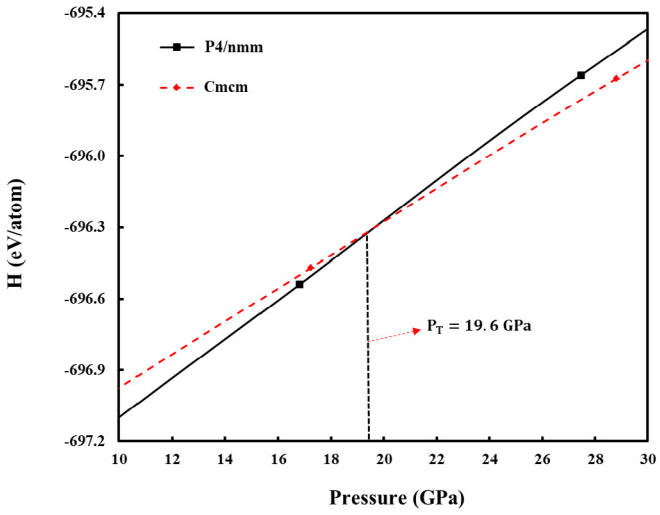

Fig. 4. (Color online) The enthalpy curves of main structural phases of BiOF.

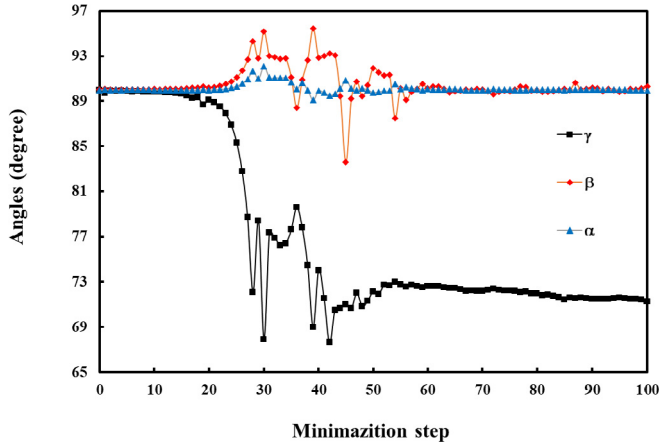

Fig. 5. (Color online) The behavior of the simulation angles (a) and cell lengths (b) as function of minimization steps at 60 GPa.

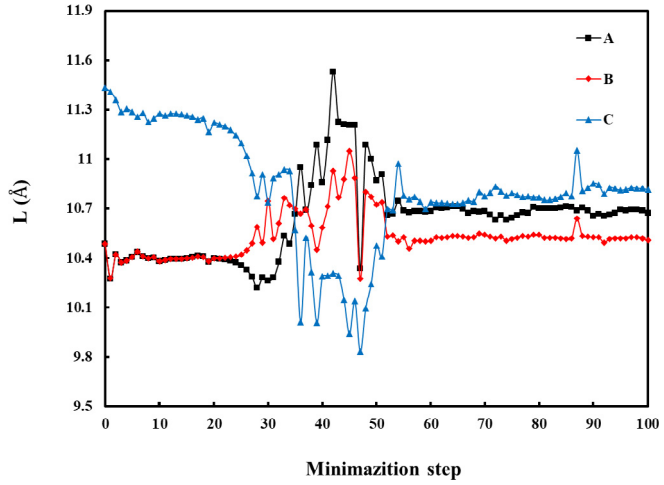

Fig. 5. (*continued*)

Each simulation step of the BiOF is analyzed in detail by the KPLOT program to determine whether there are any intermediate states during this phase change at 60 GPa. As a result of the analysis, we suggest that the Cmcm phase of BiOF proceeds through two intermediate states with space group P$\bar{1}$ at 26th step and with space group P2_1m at 44th step. The lattice constants and angles are predicted as $a = 3.4428$, $b = 3.4813$, $c = 5.5105$ Å and $\alpha = 97.2279$, $\beta = 91.7050$, $\gamma = 90.0000$ and $a = 3.6252$, $b = 3.7362$, $c = 5.1202$ Å and $\alpha = 90.0000$, $\beta = 110.7329$, $\gamma = 90.0000$ for P$\bar{1}$ and P2_1m intermediate states, respectively. These intermediate states are depicted in Fig. 6 for evolution of the Cmcm phase.

The calculated electronic band structures of Cmcm are given in Figs. 7 and 8 for P4/nmm and Cmcm phases, respectively. The density of state curves calculated for structures P4/nmm and Cmcm are given in Figs. 9 and 10, respectively, along high symmetry directions and shown at the level of Fermi energy as a function of the energy. The Fermi energy level is set to 0 eV. The symmetry points are chosen as Z– A– M– Γ– Z– R– X– Γ for the P4/nmm phase and Γ– Z– T– Y– Γ– S– R– Z for the Cmcm phase. As seen from the electronic band structure graphs, the valence band is located below the Fermi Energy level and the transmission band is located on the top. The

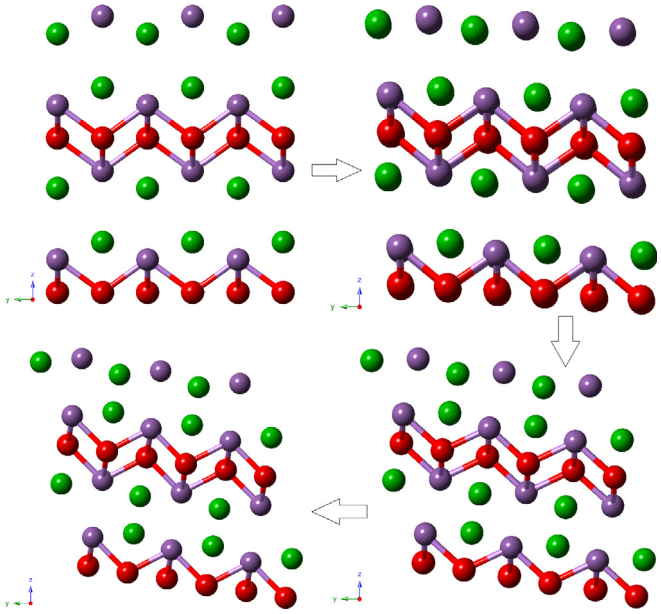

Fig. 6. (Color online) Formation of Cmcm phase at 60 GPa.

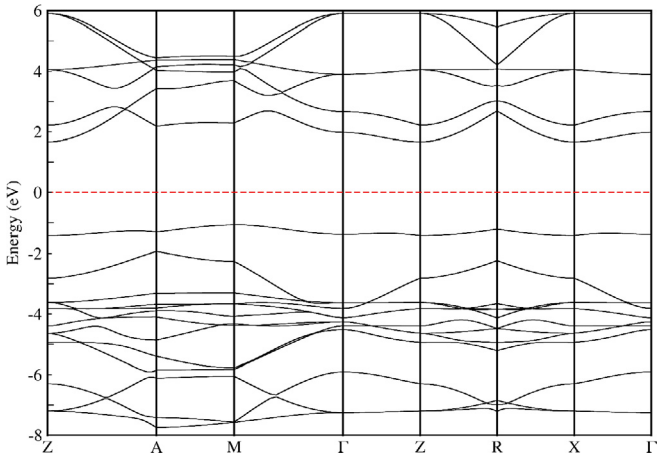

Fig. 7. (Color online) Band structure for BiOF in the P4/nmm phase at 0 GPa.

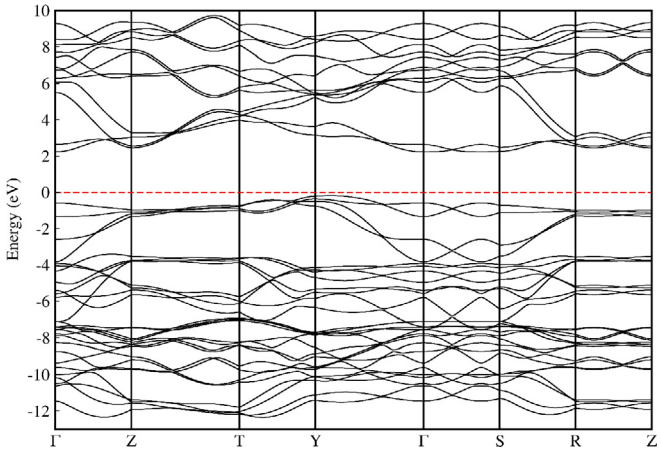

Fig. 8. (Color online) Band structure for BiOF in the Cmcm phase at 60 GPa.

obtained results show that BiOF at 0 GPa corresponds to an indirect band transition [$M \rightarrow Z$] with a band gap of about 2.74 eV. When the increasing pressure is applied to the P4/nmm phase of BiOF, a

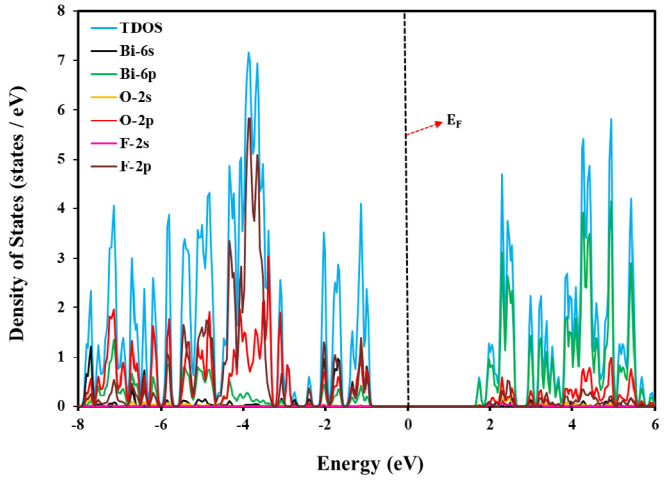

Fig. 9. (Color online) Density of states for BiOF in the P4/nmm phase at 0 GPa.

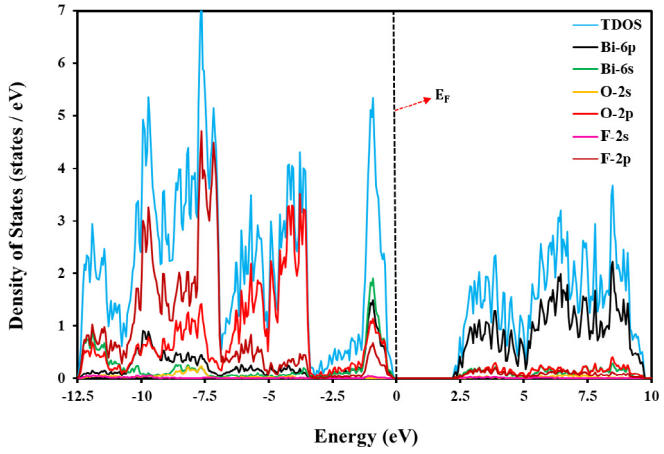

Fig. 10. (Color online) Density of states for BiOF in the Cmcm phase at 60 GPa.

transformation to the Cmcm phase was obtained. Cmcm phase of BiOF also corresponds to an indirect band transition [Y→ Γ] with a band gap of 2.47 eV. Thus, both two phases of BiOFshow semiconductor characteristic.

It is also calculated the density of states (DOS) to obtain further information about the electronic nature of BiOF and depicted in Figs. 9 and 10. It can be seen from these Figures that the largest contribution came from F-2p state between 0 - (−5), from F-2s state between −5 - (−8) and from Bi-6p state between 0 - (+6) for P4/nmm phase and from O-2p state between 0 - (−5), F-2p state between −5 - (−12.5) and Bi-6p state between 0 - (+10) for Cmcmphase.

4. Conclusions

We investigated phase transition properties of BiOF under high hydrostatic pressure using ab initio calculations. BiOF exhibits phase transition at different pressure. The phase transformation from the tetragonal PbFCl structure with space group P4/nmm to the orthorhombic structure with space group Cmcm. The predicted phase transition is also analyzed from the total energy, enthalpy calculations. In addition, the intermediate states for first time was predicted in the simulations for Cmcm phase of BiOF. We also introduced electronic properties of obtained phases of BiOFunder pressure and predicted band gaps as 2.74 and 2.47 eV for P4/nmm and Cmcm phases, respectively.

References

[1] J. Xiong, et al., Tunable BiOCl hierarchical nanostructures for high-efficient photocatalysis under visible light irradiation, Chem. Eng. J. 220 (2013) 228–236.
[2] J. Xiong, et al., Well-crystallized square-like 2D BiOCl nanoplates: mannitol-assisted hydrothermal synthesis and improved visible-light-driven photocatalytic performance, RSC Adv. 1 (8) (2011) 1542–1553.
[3] W. Fang, et al., Thermostability and photocatalytic performance of BiOCl 0.5 Br 0.5 composite microspheres, J. Mater. Res. 30 (20) (2015) 3125–3133.
[4] M. Guan, et al., Vacancy associates promoting solar-driven photocatalytic activity of ultrathin bismuth oxychloride nanosheets, J. Am. Chem. Soc. 135 (28) (2013) 10411–10417.
[5] G. Li, et al., BiOX (X= Cl, Br, I) nanostructures: mannitol-mediated microwave synthesis, visible light photocatalytic performance, and Cr (VI) removal capacity, J. Colloid Interface Sci. 409 (2013) 43–51.
[6] G. Li, et al., Facile microwave synthesis of 3D flowerlike BiOBr nanostructures and their excellent CrVI removal capacity, Eur. J. Inorg. Chem. 2012 (15) (2012) 2508–2513.
[7] H. Li, et al., Sustainable molecular oxygen activation with oxygen vacancies on the {001} facets of BiOCl nanosheets under solar light, Nanoscale 6 (23) (2014) 14168–14173.
[8] H. Li, L. Zhang, Oxygen vacancy induced selective silver deposition on the {001} facets of BiOCl single-crystalline nanosheets for enhanced Cr (VI) and sodium pentachlorophenate removal under visible light, Nanoscale 6 (14) (2014) 7805–7810.
[9] F. Tian, et al., Thickness-tunable solvothermal synthesis of BiOCl nanosheets and their photosensitization catalytic performance, New J. Chem. 39 (2) (2015) 1274–1280.
[10] L. Chen, et al., Facile synthesis of BiOCl nano-flowers of narrow band gap and their visible-light-induced photocatalytic property, Catal. Commun. 23 (2012) 54–57.
[11] K. Zhao, X. Zhang, L. Zhang, The first BiOI-based solar cells, Electrochem. Commun. 11 (3) (2009) 612–615.
[12] S. Cao, et al., A novel BiOCl film with flowerlike hierarchical structures and its optical properties, Nanotechnology 20 (27) (2009) 275702.
[13] Z. Deng, et al., From bulk metal Bi to two-dimensional well-crystallized BiOX (X= Cl, Br) micro-and nanostructures: synthesis and characterization, Cryst. Growth Des. 8 (8) (2008) 2995–3003.
[14] H. Peng, et al., Shape evolution of layer-structured bismuth oxychloride nanostructures via low-temperature chemical vapor transport, Chem. Mater. 21 (2) (2008) 247–252.
[15] D. Berlincourt, Piezoelectric ceramic compositional development, J. Acoust. Soc. Am. 91 (5) (1992) 3034–3040.
[16] K.-L. Zhang, et al., Study of the electronic structure and photocatalytic activity of the BiOCl photocatalyst, Appl. Catal. B Environ. 68 (3–4) (2006) 125–129.
[17] W. Wang, F. Huang, X. Lin, xBiOI–(1−x) BiOCl as efficient visible-light-driven photocatalysts, Scripta Mater. 56 (8) (2007) 669–672.
[18] W. Wang, et al., Visible-light-responsive photocatalysts xBiOBr–(1−x) BiOI, Catal. Commun. 9 (1) (2008) 8–12.
[19] J. Henle, et al., Nanosized BiOX (X= Cl, Br, I) particles synthesized in reverse microemulsions, Chem. Mater. 19 (3) (2007) 366–373.
[20] W.L. Huang, Electronic structures and optical properties of BiOX (X= F, Cl, Br, I) via DFT calculations, J. Comput. Chem. 30 (12) (2009) 1882–1891.
[21] W.L. Huang, Q. Zhu, Electronic structures of relaxed BiOX (X= F, Cl, Br, I) photocatalysts, Comput. Mater. Sci. 43 (4) (2008) 1101–1108.
[22] W.L. Huang, Q. Zhu, DFT calculations on the electronic structures of BiOX (X= F, Cl, Br, I) photocatalysts with and without semicore Bi 5d states, J. Comput. Chem. 30 (2) (2009) 183–190.
[23] L. Zhao, et al., First-principles study on the structural, electronic and optical properties of BiOX (X= Cl, Br, I) crystals, Phys. B Condens. Matter 407 (17) (2012) 3364–3370.
[24] H. Zhang, L. Liu, Z. Zhou, First-principles studies on facet-dependent photocatalytic properties of bismuth oxyhalides (BiOXs), RSC Adv. 2 (24) (2012) 9224–9229.
[25] H. Zhang, L. Liu, Z. Zhou, Towards better photocatalysts: first-principles studies of the alloying effects on the photocatalytic activities of bismuth oxyhalides under visible light, Phys. Chem. Chem. Phys. 14 (3) (2012) 1286–1292.
[26] D. Zhou, et al., Pressure-induced phase transition of BiOF: novel two-dimensional layered structures, Phys. Chem. Chem. Phys. 17 (6) (2015) 4434–4440.
[27] P. Ordejón, E. Artacho, J.M. Soler, Self-consistent order-N density-functional calculations for very large systems, Phys. Rev. B 53 (16) (1996) R10441.
[28] J.P. Perdew, K. Burke, M. Ernzerhof, Generalized gradient approximation made simple, Phys. Rev. Lett. 77 (18) (1996) 3865.
[29] N. Troullier, J.L. Martins, Efficient pseudopotentials for plane-wave calculations, Phys. Rev. B 43 (3) (1991) 1993.
[30] H.J. Monkhorst, J.D. Pack, Special points for Brillouin-zone integrations, Phys. Rev. B 13 (12) (1976) 5188.
[31] R. Hundt, et al., Determination of symmetries and idealized cell parameters for simulated structures, J. Appl. Crystallogr. 32 (3) (1999) 413–416.
[32] A. Hannemann, et al., A new algorithm for space-group determination, J. Appl. Crystallogr. 31 (6) (1998) 922–928.
[33] C. Yamcicier, Z. Merdan, C. Kurkcu, Investigation of the structural and electronic properties of CdS under high pressure: an ab initio study, Can. J. Phys. 96 (2) (2017) 216–224.
[34] H. Öztürk, M. Durandurdu, High-pressure phases of ZrO 2: an ab initio constant-pressure study, Phys. Rev. B 79 (13) (2009) 134111.
[35] C. Kürkçü, Z. Merdan, H. Öztürk, Theoretical calculations of high-pressure phases of NiF 2: an ab initio constant-pressure study, Russ. J. Phys. Chem. A 90 (13) (2016) 2550–2555.
[36] C. Kürkçü, Z. Merdan, H. Öztürk, Pressure-induced phase transitions and structural properties of CoF2: an ab-initio molecular dynamics study, Solid State Commun. 231 (2016) 17–25.
[37] F. Birch, Finite elastic strain of cubic crystals, Phys. Rev. 71 (11) (1947) 809.
[38] F. Murnaghan, The compressibility of media under extreme pressures, Proc. Natl. Acad. Sci. Unit. States Am. 30 (9) (1944) 244–247.
[39] Z. Yang, et al., First-principles calculations of the vacancy defects in BiOF as cathode materials for Li-ion batteries, Comput. Mater. Sci. 74 (2013) 50–54.
[40] S. Li, et al., Electronic structural properties of BiOF crystal and its oxygen vacancy from first-principles calculations, Russ. J. Phys. Chem. A 91 (12) (2017) 2425–2430.
[41] W.L. Huang, Q. Zhu, Electronic structures of relaxed BiOX (X=F, Cl, Br, I) photocatalysts, Comput. Mater. Sci. 43 (4) (2008) 1101–1108.
[42] H. Zhang, L. Liu, Z. Zhou, Towards better photocatalysts: first-principles studies of the alloying effects on the photocatalytic activities of bismuth oxyhalides under visible light, Phys. Chem. Chem. Phys. 14 (3) (2012) 1286–1292.
[43] W.L. Huang, Electronic structures and optical properties of BiOX (X = F, Cl, Br, I) via DFT calculations, J. Comput. Chem. 30 (12) (2009) 1882–1891.
[44] G. Wang, et al., BiOX/BiOY (X, Y = F, Cl, Br, I) superlattices for visible light photocatalysis applications, RSC Adv. 6 (94) (2016) 91508–91516.
[45] A.M. Ganose, et al., Interplay of orbital and relativistic effects in bismuth oxyhalides: BiOF, BiOCl, BiOBr, and BiOI, Chem. Mater. 28 (7) (2016) 1980–1984.